ETH
Eidgenössische Technische Hochschule Zürich
Swiss Federal Institute of Technology Zurich

Department of Physics
Laboratory for Solid State Physics
Quantum Device Lab

Semester Thesis

Optimization of the microwave properties of a cryostat sample holder

Silvio Marx

Zurich
June & July 2009

Supervisor Dr. Stefan Filipp
Group Leader Prof. Dr. Andreas Wallraff

Contents

1. Introduction

Since the early days of the transistor a tremendous development has taken place. That incorporates shrinking of the transistor over several orders of magnitude, implementing advanced calculation methods and increasing the operation frequency. This led to millions and sometimes even billions of transistors working together with a rate of some GHz. The high calculation speed of personal computers has a big impact on our daily life since together with connecting many of them together via large networks gives nearly 'infinite possibilities'.

Nevertheless, every architecture has its limits and therefore specialized new approaches will be developed to avoid them, possibly giving promising new applications in the future. The new approach wants to make use of other laws of physics, namely quantum mechanics. The old concept of the bit as a two level system with only two possible states will be replaced by the quantum bit, qubit in short. This is a two level system in which the quantum bit can exist not only in one of the two states but also in an arbitrary superposition of them. With such a system new algorithms can be implemented which speed up calculations for specialized tasks enormously. There are three classes of applications that profit from the new possibilities so far. They are the Quantum Fourier Transformation, Quantum Search Algorithms and Quantum Simulation, see subsection 'Quantum Algorithms' in [1, p. 28 ff.] for details.

To make use of the fragile quantum bit, environmental effects on its state must be suppressed as much as possible. One of those effects is thermal noise and therefore one cools down the qubit as much as possible which is nowadays of the order of mK. The qubit is mounted on a chip and on top of the chip is a sample holder whereas the sample holder itself is placed in a cryostat. The sample holder is a metal box which forms a cavity for microwave photons. They are used to prepare the qubit states, applying the microwave pulses necessary for the experiment and read out the final states. Such a microwave cavity acts as a cavity resonator and possibly influences the state of the qubit in the experiment. To avoid this, the semester thesis' goal is to optimize the geometry of the sample holder in designing a new cover for the sample.

The main idea behind the optimization is to fill out the sample holder cavity as much as possible with a conducting material. This should shift possible resonance frequencies beyond 20 GHz where they couple considerably less to the qubits. Therefore the existing chip cover was redesigned and with measurements the effects where evaluated. In particular this means the cover was increased in height as much as possible and the space directly above the chip was changed to measure the influence of this parameter. Measurements showed that the biggest effect was due to the increased height. Further changes did not have a significant effect at least up to about 15 GHz despite the frequency shift of the qubit when the chip cover was closer to the chip.

2. Theory

2.1. Introduction

In this section measurement parameters needed to characterize the electronic circuit are explained. Furthermore, a derivation of resonance frequencies for cavity resonators is given based on Maxwell's equations for electromagnetism to understand the behavior of the microwaves in the sample holder. If this is successfully compared with measurement data we would know where the unwanted resonances come from and therefore be able to optimize the sample holder. For comparison of the calculated formulas derived in this chapter with the experimental data see chapter 5.

2.2. Scattering parameters

Since in the following measurements the so called scattering parameters will appear, there is a need to introduce them first. The following discussion is based on [2, p. 174 ff.].

For an N-port electronic network to be fully characterized one needs N^2 parameters for any frequency since the ports can measure transmission and reflection of signals. One way of characterizing the behavior of the electronics is to use a network analyzer device like the one used in this thesis, see figure 4.1. The network analyzer is capable of determining all the parameters for the desired characterization in a relatively short amount of time. The complete characterization can be done in many ways, one is to use the scattering matrix. It is a description of the amplitude of the voltage wave V_n^- reflected from port n in terms of the amplitude of the voltage wave V_n^+ incident on port n. The scattering matrix S is defined as

$$\begin{bmatrix} V_1^- \\ V_2^- \\ \vdots \\ V_N^- \end{bmatrix} = \begin{bmatrix} S_{11} & S_{12} & \cdots & S_{1N} \\ S_{21} & \ddots & & \vdots \\ \vdots & & & \\ S_{N1} & S_{N2} & \cdots & S_{NN} \end{bmatrix} \begin{bmatrix} V_1^+ \\ V_2^+ \\ \vdots \\ V_N^+ \end{bmatrix}$$

or equivalently

$$\left[V^-\right] = [S]\left[V^+\right]. \tag{2.1}$$

For determining the matrix elements S_{ij} the following formula should be used

$$S_{ij} = \frac{V_i^-}{V_j^+}\Big|_{V_k^+ = 0 \text{ for } k \neq j} \tag{2.2}$$

2.3. Cavity resonators and waveguides

In general the concept of a resonator is a system which oscillates naturally at a specific frequency, called its resonance frequency. The oscillation can be mechanical or electromagnetic, here we have an electromagnetic oscillation. Microwave photons are reflected by the metal of the sample holder like optical light by a mirror. Therefore in a cavity a standing wave is formed, a non-traveling wave with oscillating amplitude. The electromagnetic amplitude can now couple to the parts on the chip and influence their state.

The copper sample holder analyzed here can be modeled by a cylindrical cavity resonator and the cavity above the resonator chips and the signal lines by a rectangular box resonator. For the understanding of the behavior of the sample together with the sample holder it is necessary to know what resonance frequencies can appear in such geometries. This can be done by analyzing a general waveguide and then closing its ends, imposing further boundary conditions. To know about the electric and magnetic fields one has to solve Maxwell's equations with the boundary condition that the tangential component of the electric field E_t vanishes on the walls of the resonator. This is because E_t must be continuous across different media and the material of the cover has a comparatively high conductivity, assumed here to be infinitely large. That means the penetration depths goes to zero which means vanishing electric field inside the material. A complete treatment of this can be found in [2] at pages 92 ff. and 278 ff.

2.3.1. General treatment

Suppose we are given an arbitrary waveguide, filled with material described with the electromagnetic parameters permittivity ϵ and permeability μ. Furthermore, we assume time-harmonic fields $\mathbf{E}$ and $\mathbf{H}$ with $e^{i\omega t}$ dependence (omitted here) such that:

$$\mathbf{E}(x,y,z) = [\mathbf{e}(x,y) + \mathbf{z}e_z(x,y)]\, e^{-i\beta z} \tag{2.3}$$

$$\mathbf{H}(x,y,z) = [\mathbf{h}(x,y) + \mathbf{z}h_z(x,y)]\, e^{-i\beta z}, \tag{2.4}$$

where $\mathbf{e}$(x,y) and $\mathbf{h}$(x,y) represent the transverse electric and magnetic fields while e_z and h_z are the longitudinal electric and magnetic components of the fields and β is a wavenumber.

If the waveguide or the cavity resonator does not contain sources of the fields $\mathbf{E}$ and $\mathbf{H}$ the Maxwell equations read

$$\nabla \times \mathbf{E} = -i\omega\mu\mathbf{H} \qquad and \tag{2.5}$$

$$\nabla \times \mathbf{H} = i\omega\epsilon\mathbf{E}. \tag{2.6}$$

Neglecting the $e^{-i\beta z}$ component for the moment, one can write the following six equations for the field components

$$\frac{\partial E_z}{\partial y} + i\beta E_y = -i\omega\mu H_x \tag{2.7}$$

$$-\frac{\partial E_z}{\partial x} - i\beta E_x = -i\omega\mu H_y \tag{2.8}$$

$$\frac{\partial E_y}{\partial x} - \frac{\partial E_x}{\partial y} = -i\omega\mu H_z \tag{2.9}$$

$$\frac{\partial H_z}{\partial y} + i\beta H_y = i\omega\epsilon E_x \tag{2.10}$$

$$-\frac{\partial H_z}{\partial x} - i\beta H_x = i\omega\epsilon E_y \tag{2.11}$$

$$\frac{\partial H_y}{\partial x} - \frac{\partial H_x}{\partial y} = i\omega\epsilon E_z \tag{2.12}$$

These equations can be solved for the transverse in terms of the longitudinal components as follows

$$H_x = \frac{i}{k_c^2}\left(\omega\epsilon\frac{\partial E_z}{\partial y} - \beta\frac{\partial H_z}{\partial x}\right) \tag{2.13}$$

$$H_y = \frac{-i}{k_c^2}\left(\omega\epsilon\frac{\partial E_z}{\partial x} + \beta\frac{\partial H_z}{\partial y}\right) \tag{2.14}$$

$$E_x = \frac{-i}{k_c^2}\left(\beta\frac{\partial E_z}{\partial x} + \omega\mu\frac{\partial H_z}{\partial y}\right) \tag{2.15}$$

$$E_y = \frac{i}{k_c^2}\left(-\beta\frac{\partial E_z}{\partial y} + \omega\mu\frac{\partial H_z}{\partial x}\right) \tag{2.16}$$

$$k_c^2 = k^2 - \beta^2 \tag{2.17}$$

where k_c is the so called cutoff wavenumber. For wavenumbers $k \ll k_c$ the amplitude of the field is significantly reduced. In the following subsections the general results will be applied for specific cases. Transverse electric and magnetic modes are calculated.

2.3.2. Box resonators

The box resonator is treated as a special rectangular waveguide and the direction of propagation is **z** with dimension 'd'. Along **x** and **y** direction it has dimensions 'a' and 'b'. For calculating the resonance frequencies of the resonator we consider first a waveguide and close and short it on the ends in **z** direction.

TE and TM modes

Transverse electric - TE - modes for a rectangular waveguide have the property that their longitudinal component $E_z = 0$ but $H_z \neq 0$. Using these conditions, H_z must fulfill the

reduced Helmholtz wave equation

$$\left(\frac{\partial^2}{\partial x^2}+\frac{\partial^2}{\partial y^2}+k_c^2\right)h_z(x,y)=0 \tag{2.18}$$

with $H_z(x,y,z)=h_z(x,y)e^{-i\beta z}$. Using the method of separation of variables and the boundary condition that the electric field component tangential to the waveguide walls must vanish one can solve the problem. This leads to

$$e_x(x,y)=0 \qquad at\ y=0,b \tag{2.19}$$

$$e_y(x,y)=0 \qquad at\ x=0,a. \tag{2.20}$$

In the case of TM modes this is sufficient also for the e_z component to vanish at the walls. One can find the solution for H_z

$$H_z(x,y,z)=A_{mn}\cos\left(\frac{m\pi x}{a}\right)\cos\left(\frac{n\pi y}{b}\right)e^{-i\beta z} \tag{2.21}$$

which leads with equations 2.13 to 2.16 to the following solution for the transverse components

$$E_x=\frac{i\omega\mu n\pi}{k_c^2 b}A_{mn}\cos\left(\frac{m\pi x}{a}\right)\sin\left(\frac{n\pi y}{b}\right)e^{-i\beta z}, \tag{2.22}$$

$$E_y=\frac{-i\omega\mu m\pi}{k_c^2 a}A_{mn}\sin\left(\frac{m\pi x}{a}\right)\cos\left(\frac{n\pi y}{b}\right)e^{-i\beta z}, \tag{2.23}$$

$$H_x=\frac{i\beta m\pi}{k_c^2 a}A_{mn}\sin\left(\frac{m\pi x}{a}\right)\cos\left(\frac{n\pi y}{b}\right)e^{-i\beta z}, \tag{2.24}$$

$$H_y=\frac{i\beta n\pi}{k_c^2 b}A_{mn}\cos\left(\frac{m\pi x}{a}\right)\sin\left(\frac{n\pi y}{b}\right)e^{-i\beta z} \tag{2.25}$$

and propagation constant

$$\beta=\sqrt{k^2-k_c^2} \tag{2.26}$$

with

$$k_c=\sqrt{\left(\frac{m\pi}{a}\right)^2+\left(\frac{n\pi}{b}\right)^2} \tag{2.27}$$

leads to

$$\beta_{mn}=\sqrt{k^2-\left(\frac{m\pi}{a}\right)^2-\left(\frac{n\pi}{b}\right)^2}. \tag{2.28}$$

Imposing finally the boundary conditions in the **z** direction, to form a rectangular box resonator,

$$E_x(z=0)=E_x(z=d)=E_y(z=0)=E_y(z=d)=0, \tag{2.29}$$

and using the previous result for transverse fields E_x and E_y from equations 2.22 and 2.23 E_t can be expressed as

$$E_t(x,y,z) = \mathbf{e}(x,y)\left[A^+ e^{-i\beta_{mn}z} + A^- e^{i\beta_{mn}z}\right]. \tag{2.30}$$

Here, $\mathbf{e}$(x,y) is the transverse variation of the mode and A^+ and A^- are arbitrary amplitudes of the forward and backward traveling waves in the resonator. Applying the boundary conditions at the walls gives the two equations

$$A^+ = -A^- \tag{2.31}$$

$$E_t(x,y,d) = -\mathbf{e}(x,y)A^+ 2i\sin(\beta_{mn}d) = 0. \tag{2.32}$$

The only nontrivial solutions ($A^+ \neq 0$) occur for

$$\beta_{mn}d = l\pi \qquad\qquad l = 0,1,2,... \tag{2.33}$$

The rectangular cavity is thus a waveguide version of a $\lambda/2$ transmission line resonator. With equations 2.28 and 2.33 one can define a resonant wavenumber for the TE_{mnl} mode

$$k_{mnl} = \sqrt{\left(\frac{m\pi}{a}\right)^2 + \left(\frac{n\pi}{b}\right)^2 + \left(\frac{l\pi}{d}\right)^2} \tag{2.34}$$

and a resonant frequency

$$f_{nml} = \frac{ck_{mnl}}{2\pi\sqrt{\mu_r\epsilon_r}} = \frac{c}{2\sqrt{\mu_r\epsilon_r}}\sqrt{\left(\frac{m}{a}\right)^2 + \left(\frac{n}{b}\right)^2 + \left(\frac{l}{d}\right)^2}. \tag{2.35}$$

An analogous result holds for the TM_{mnl} modes which give the same resonant frequencies.

2.3.3. Cylindrical resonators

Like the rectangular box waveguide the cylindrical version of it guides TE and TM modes, too. So we are given a hollow metal cylinder with radius 'a'. The resonator is then the terminated version of the waveguide with a length 'd' in **z** direction.

TE modes

Following the arguments from subsection 2.3.1 about the general treatment of waveguides one can derive the transverse fields from the longitudinal ones. Since cylindrical symmetry is involved we change to the corresponding coordinate system. The dependences are as follows

$$E_\rho = \frac{-i}{k_c^2}\left(\beta\frac{\partial E_z}{\partial\rho} + \frac{\omega\mu}{\rho}\frac{\partial H_z}{\partial\phi}\right), \tag{2.36}$$

$$E_\phi = \frac{-i}{k_c^2}\left(\frac{\beta}{\rho}\frac{\partial E_z}{\partial\phi} - \omega\mu\frac{\partial H_z}{\partial\rho}\right), \tag{2.37}$$

$$H_\rho = \frac{i}{k_c^2}\left(\frac{\omega\epsilon}{\rho}\frac{\partial E_z}{\partial \phi} - \beta\frac{\partial H_z}{\partial \rho}\right), \tag{2.38}$$

$$H_\phi = \frac{-i}{k_c^2}\left(\omega\epsilon\frac{\partial E_z}{\partial \rho} + \frac{\beta}{\rho}\frac{\partial H_z}{\partial \phi}\right) \tag{2.39}$$

with the propagation factor of $e^{-i\beta z}$ and a cutoff wavenumber $k_c^2 = k^2 - \beta^2$.

As before the TE mode is defined by $E_z = 0$ while $H_z \neq 0$. Then $H_z(\rho, \phi, z) = h_z(\rho, \phi)e^{-i\beta z}$ must obey the wave equation

$$\left(\nabla^2 + k^2\right) H_z = 0 \tag{2.40}$$

and in cylindrical coordinates

$$\left(\frac{\partial^2}{\partial \rho^2} + \frac{1}{\rho}\frac{\partial}{\partial \rho} + \frac{1}{\rho^2}\frac{\partial^2}{\partial \phi^2} + k_c^2\right) h_z(\rho, \phi) = 0 \tag{2.41}$$

The general solution is

$$h_z(\rho, \phi) = \left[A\sin(n\phi) + B\cos(n\phi)\right] J_c(k_c\rho) \tag{2.42}$$

with $J_c(k_c\rho)$ the Bessel function of first kind. Still the cutoff wavenumber has to be calculated. Therefore we impose the boundary condition of the vanishing tangential component of $\mathbf{E}$ which means that

$$E_\phi(\rho, \phi) = 0 \qquad\qquad at\ \rho = a. \tag{2.43}$$

Since

$$E_\phi(\rho, \phi, z) = \frac{i\omega\mu}{k_c}\left[A\sin(n\phi) + B\cos(n\phi)\right] J_n'(k_c\rho)e^{-i\beta z}, \tag{2.44}$$

where $J_n'(k_c\rho)$ is the derivative of the Bessel function of first kind with respect to its argument. After equation 2.43

$$J_n'(k_c a) = 0 \tag{2.45}$$

must hold. The roots of J_n' are named p_{nm}' such that $J_n'(p_{nm}') = 0$ and must be evaluated numerically, n are the circumferential variations and m are the radial variations. The propagation constant of the TE_{nm} mode is

$$\beta_{nm} = \sqrt{k^2 - k_c^2} = \sqrt{k^2 - \left(\frac{\rho_{nm}'}{a}\right)^2}. \tag{2.46}$$

The general solution for the TE modes are then

$$E_\phi = \frac{i\omega\mu}{k_c}\left[A\sin(n\phi) + B\cos(n\phi)\right] J_n'(k_c\rho)e^{-i\beta z}, \tag{2.47}$$

$$E_\rho = \frac{-i\omega\mu n}{k_c^2\rho}\left[A\cos(n\phi) - B\sin(n\phi)\right] J_n(k_c\rho)e^{-i\beta z}, \tag{2.48}$$

$$H_\phi = \frac{-i\beta n}{k_c^2\rho}\left[A\cos(n\phi) - B\sin(n\phi)\right] J_n(k_c\rho)e^{-i\beta z}, \tag{2.49}$$

$$H_\rho = \frac{-i\beta}{k_c}\left[A\sin(n\phi) + B\cos(n\phi)\right] J_n'(k_c\rho)e^{-i\beta z}. \tag{2.50}$$

As before we can write the transverse components E_ρ and E_ϕ of the field $\mathbf{E}$ as

$$E_t(\rho,\phi,z) = \mathbf{e}(\rho,\phi)\left(A^+e^{-i\beta_{nm}z} + A^-e^{i\beta_{nm}z}\right), \tag{2.51}$$

where $\mathbf{e}(\rho,\phi)$ is the transverse variation of the mode and A^+ and A^- are arbitrary amplitudes of the forward and backward traveling waves in the resonator.
Imposing the boundary condition

$$E_t = 0 \qquad\qquad at\ z = 0, d \tag{2.52}$$

leads to $A^+ = -A^-$ and

$$A^+\sin(\beta_{nm}d) = 0 \tag{2.53}$$

with solutions

$$\beta_{nm}d = l\pi \qquad\qquad for\ l = 0, 1, 2, ... \tag{2.54}$$

Together with equation 2.46 the resonant frequencies of the TE_{nml} are

$$f_{nml} = \frac{c}{2\pi\sqrt{\mu_r\epsilon_r}}\sqrt{\left(\frac{p'_{nm}}{a}\right)^2 + \left(\frac{l\pi}{d}\right)^2}. \tag{2.55}$$

TM modes

The transverse magnetic modes are derived in analogy to the previous subsection, just with $H_z = 0$ and $E_z \neq 0$. Imposing the boundary condition

$$E_z(\rho,\phi) = \left[A\sin(n\phi) + B\cos(n\phi)\right] J_n(k_c\rho)e^{-i\beta z} = 0 \quad for\ \rho = a \tag{2.56}$$

it follows that

$$J_n(k_ca) = 0 \tag{2.57}$$

or

$$k_c = \frac{p_{nm}}{a} \tag{2.58}$$

with $J_n(p_{nm}) = 0$. The propagation constant of the TM_{nm} mode is

$$\beta_{nm} = \sqrt{k^2 - k_c^2} = \sqrt{k^2 - \left(\frac{p_{nm}}{a}\right)^2}. \tag{2.59}$$

The solution for the transverse fields are then

$$E_\phi = \frac{-i\beta n}{k_c^2 \rho} \left[A\cos(n\phi) - B\sin(n\phi)\right] J_n(k_c\rho) e^{-i\beta z}, \tag{2.60}$$

$$E_\rho = \frac{-i\beta}{k_c} \left[A\sin(n\phi) + B\cos(n\phi)\right] J_n'(k_c\rho) e^{-i\beta z}, \tag{2.61}$$

$$H_\phi = \frac{-i\omega\epsilon}{k_c} \left[A\sin(n\phi) + B\cos(n\phi)\right] J_n'(k_c\rho) e^{-i\beta z}, \tag{2.62}$$

$$H_\rho = \frac{i\omega\epsilon n}{k_c^2 \rho} \left[A\cos(n\phi) - B\sin(n\phi)\right] J_n(k_c\rho) e^{-i\beta z}. \tag{2.63}$$

From the TE modes we know that $\beta_{nm} d = l\pi$ such that together with equation 2.59 we end up with the resonance frequencies of the TM_{nml} modes

$$f_{nml} = \frac{c}{2\pi\sqrt{\mu_r \epsilon_r}} \sqrt{\left(\frac{p_{nm}}{a}\right)^2 + \left(\frac{l\pi}{d}\right)^2}. \tag{2.64}$$

2.4. Summary

From the calculation of the resonance frequencies one notices that there is a smallest frequency determined by the cutoff wavenumber k_c. Any frequency below is significantly damped. For cylindrical resonators these are basically determined by the radius of the cylinder, for box resonators by the width and the height of the box. These dimensions are for the sample holder on the order of several cm, therefore the lowest resonance frequency is in the range of several GHz. Since the spectral range of interest is up to about 20 GHz we expect that these frequencies might appear in our spectrum. For the exact geometry the numbers are calculated in chapter 5 and compared to the measurements.

3. Cover Design

3.1. Introduction

As mentioned in the introduction, the measurement setup is basically a microwave resonator chip mounted on top of a PCB where qubits are placed in positions with high field amplitude. This PCB is contained in a metallic sample holder box inside a cryostat that cools the chip to several mK. The design used for the sample holder box can be seen in figure 3.1. The experiments are done with microwaves that are brought to the chip via coaxial cables. Since microwaves from the coaxial lines terminated on the chip can leak out, distribute in the sample holder box and form standing waves that can couple to the qubits. At which frequencies these standing waves might be we have calculated in the previous chapter. We have seen that they depend on the specific geometry of the sample holder which we want to change to improve the experiment. In this chapter the designing is described together with measurements that motivate the changes.

3.2. 3D modeling software

For modeling the PCB cover in 3D, the software Autodesk® Inventor™ Professional 2009 was chosen because it is a powerful tool for this purpose and the model of the previous version from Dr. Stefan Filipp was already in this format. This made it relatively easy to create a new version of the cover that improves the microwave properties of the cryostat sample holder.

3.3. The previous cover design

The previous cover is geared to a typical PCB layout which is most compatible to the existing samples. It must fit inside the sample holder, which is 4.8 mm in height and 28.5 mm in diameter, see figure 3.1. It is designed as a copper cylinder with 2.5 mm height and with cavities where necessary. This means that it has eight holes for the maximum number of eight connectors to the chip, even if they are not used. Furthermore, there are eight holes for the screws that fix it and a cavity directly above the chip and the signal lines to not damage them or to connect parts of it to ground potential.

When measurements are taken with or without this version of the cover one observes a number of peaks, see figure 3.2. Some of them are known to be from the sample, but there are also peaks that were not expected. They are thought to be resonances from remaining cavities in the sample holder box. Therefore a measurement was taken with two of these covers on top of each other to fill the remaining space inside the sample holder box. The result was very

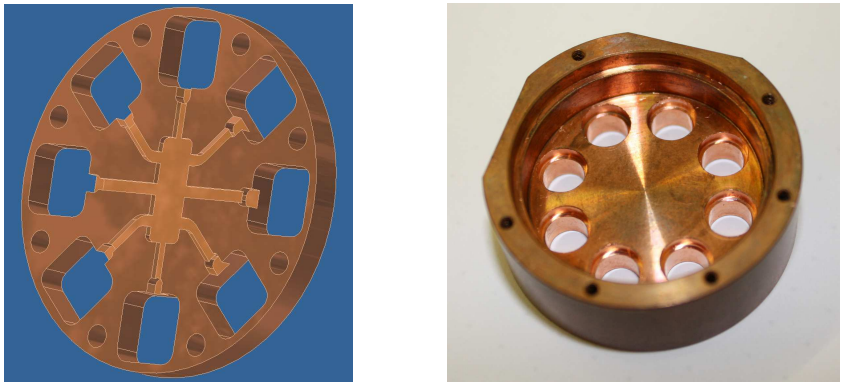

Figure 3.1.: The bottom view of the previous cover design and the top lid of the sample holder where the cover must fit in.

promising since as you can see in figure 3.2 the two big unwanted resonances at frequencies near B and D disappear. Therefore it is obvious that these peaks are cavity modes. The blue curve indicates the transmission coefficient for the very first sample holder without any cover in the sample holder cavity. The red curve has the previous cover on top of the PCB and the chip, the yellow one has two of the previous covers on top of each other to nearly fill out the complete cavity. As one can clearly see the single cover does not sufficiently damp the unwanted resonances, so there is need for improvement. The frequencies near A, C and E in figure 3.2 are the resonances of the used copper resonator, where C and E are higher harmonics of A. These resonance peaks are slightly shifted upwards in frequency when using a cover. While the peaks B and D are clearly well suppressed, the behavior of F is more complicated and not understood.

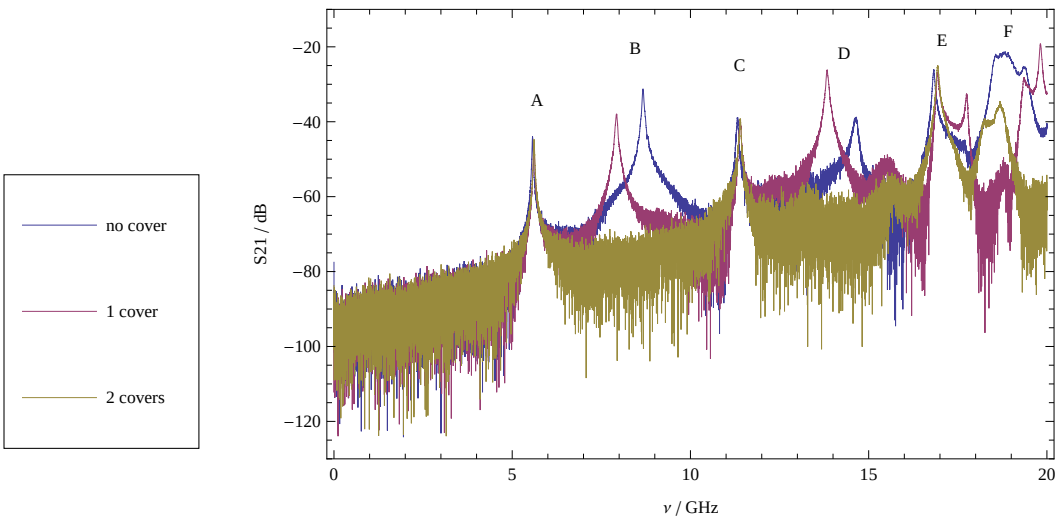

Figure 3.2.: Measurements of the transmission coefficient S21 for a copper resonator at 4 Kelvin.

In figure 3.3 you can see the transmission spectrum of the superconducting niobium resonator Tr07 at 4 Kelvin. The discussion from above seems to apply here qualitatively too. This indicates that the unexpected resonances are not a property of the sample itself but from the sample holder. The first resonance A from the niobium resonator can be observed as well as

letter	no cover		1 cover		2 covers	
	ν/GHz	S21/dB	ν/GHz	S21/dB	ν/GHz	S21/dB
A	5.5702	-43.9333	5.6092	-45.5169	5.6122	-44.6667
B	8.6672	-31.3275	7.9272	-37.9014		
C	11.322	-38.8172	11.397	-39.8851	11.398	-39.1693
D	14.654	-38.6980	13.833	-26.1867		
			15.524	-48.7529	15.531	-53.4134
E	16.829	-26.0456	16.932	-26.6628	16.935	-24.9890
			17.755	-32.7201		
F	18.830	-21.2941	18.696	-51.3566	18.684	-34.4674
F	19.346	-25.2263	19.364	-28.1818		
F			19.821	-19.3526		

Table 3.1.: Interesting peaks from figure 3.2.

the first two harmonics near C and E. Again for higher frequencies the spectrum is not as clean as at lower frequencies and the bigger peaks near B and D disappear when filling the cavity with two covers.

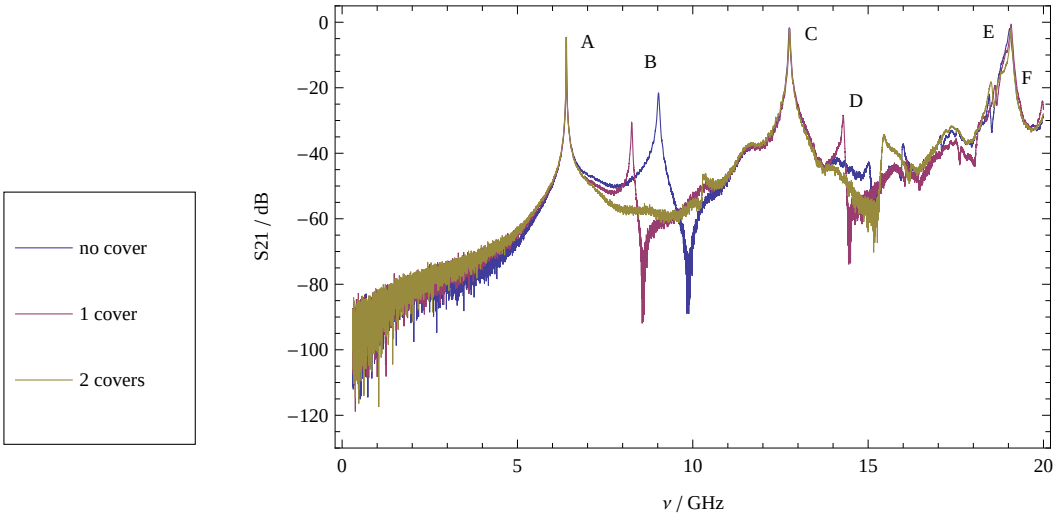

Figure 3.3.: Measurements of the transmission coefficient S21 for the niobium resonator Tr07 at 4 Kelvin.

3.4. The new cover design

As discussed in the previous section, there is need for improvement of the existing sample holder and cover design. This is the case since the unwanted resonances that occur might couple to qubits on the chip. This could influence or destroy the state of a qubit, possibly induce a decay or excite it from the ground state. Therefore they must be removed or damped as much as possible.

letter	no cover		1 cover		2 covers	
	ν/GHz	S21/dB	ν/GHz	S21/dB	ν/GHz	S21/dB
A	6.39321	-4.49620	6.39814	-4.63459	6.39223	-4.71325
B	9.02316	-21.5655	8.25979	-30.6239		
C	12.7494	-1.74568	12.7632	-1.87508	12.7593	-2.06459
D	15.0149	-42.6353	14.2900	-28.3082	15.4473	-34.1537
	16.0019	-36.9988				
	18.4545	-22.1060	18.6141	-19.2551	18.4989	-18.3008
E	19.0426	-1.94777	19.0761	-0.61734	19.0761	-1.88460
F			19.9714	-24.0523		

Table 3.2.: Interesting peaks from figure 3.3.

From the initial test with two covers on top of each other it can be concluded that it is desirable to have a single cover with the full height of the sample holder cavity. This is done as you can see in figure 3.4. The cover height increases from the initial 2.5mm to now 4.8mm, the full height of the cavity. This modification is expected to give a suppression of unwanted resonances in a frequency range up to about 16 GHz.

Other changes could include the size of the cavity around the eight connectors to the chip or the size of the cavity above the chip and the signal lines since they act as a cavity resonator, too. The corresponding frequencies however should lie at relatively high frequencies, possibly out of the spectrum since the size is so small. This can be understood well in terms of the previously mentioned cutoff frequency, the smallest allowed frequency depending on the geometry of the resonator. Since the cover is now as high as the sample holder cavity, the screw holes need to be counter-sunk such that the screw heads lie flush with the top of the cover.

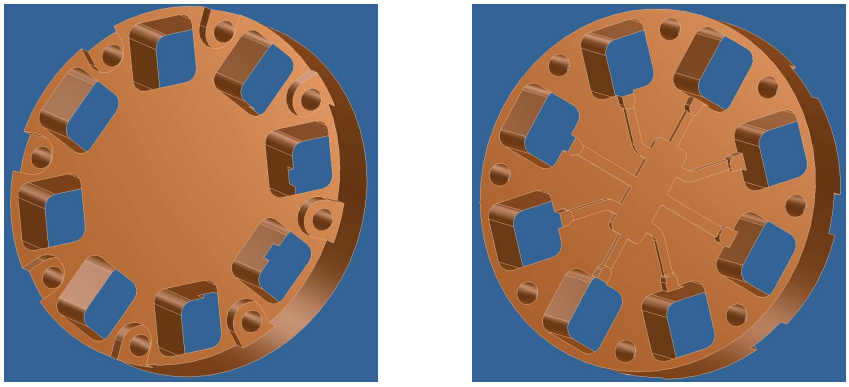

Figure 3.4.: 3D model of the new cover, top and bottom view.

The easiest and most reasonable change should then be the height of the cavity above the chip and the signal lines. They are varied as mentioned in figure 3.5 to see their influence on the spectrum. There you can also see the manufactured version made by the workshop of the physics department.

Figure 3.5.: All three covers made from oxygen-free high thermal conductivity 'OFHC' copper, differing only in the height of the cavity above the chip and signal lines. They are from left to right: 0.8mm, 0.5mm and 0.2mm

.

4. Measurements

4.1. Introduction

Referring to the theory in chapter 2 we now measure the scattering matrix of the electronic circuit. The most important matrix element S_{ij} from the scattering matrix is in this case for a 2-port network the transmission coefficient S_{21}, if the circuit is symmetric, then this equals S_{12}. Its frequency dependence is measured with different samples and configurations of the sample holder of the cryostat. From its frequency dependence and the known geometry conclusions can be drawn.

4.2. Measurement setup

The setup contains as the main measuring device the Agilent® N5230C Network Analyzer to record the spectrum. For reaching the low temperature necessary to bring the niobium resonator to the superconducting state, the sample is put into the sample holder, with or without the cover. Mounted at the end of a dip stick it is then put into a liquid helium vessel. The resulting temperature of the sample is then about 4 Kelvin. Both devices can be seen in figure 4.1.

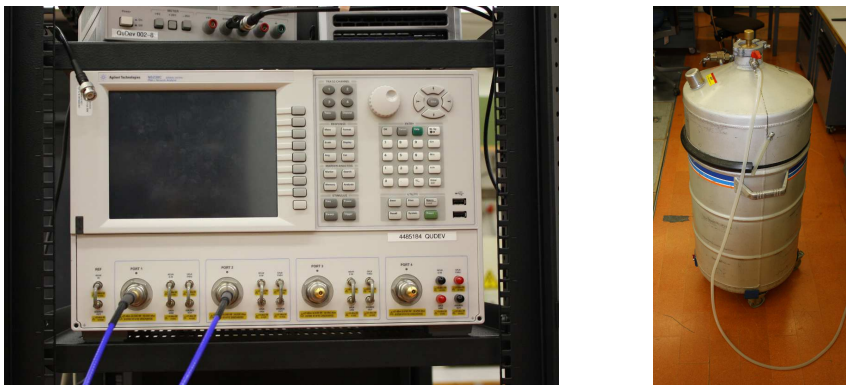

Figure 4.1.: Main measuring device: Agilent® N5230C Network Analyzer with a liquid helium vessel.

A photograph of the niobium resonator Tr07 can be seen in figure 4.2.

4.3. Measurement data

The three covers are tested with three different samples: one copper resonator and two superconducting niobium resonators Tr07 and Tr01, see figures 4.4, 4.5 and 4.6. In order to

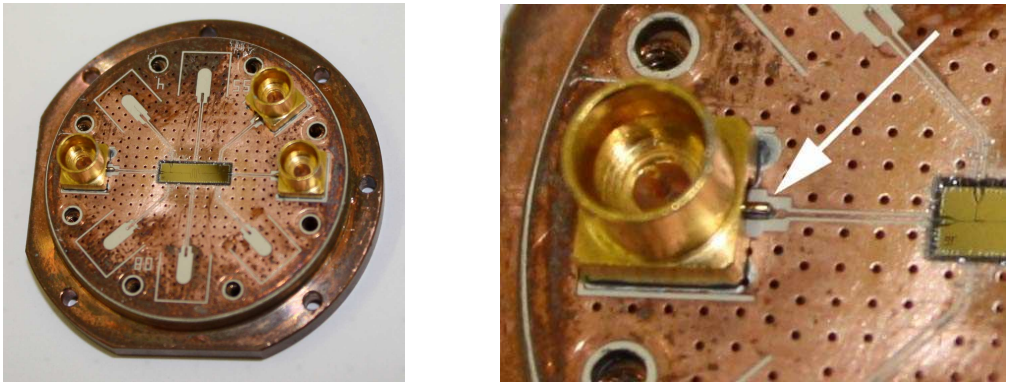

Figure 4.2.: Niobium resonator mounted on a PCB. On the right the position of the signal insertion to the PCB is indicated. This small bare cable is thought of as acting like an antenna emitting radiation into the sample holder.

obtain an absolute scale for the transmission the data must be calibrated, since the influence of the cables should not be visible in the spectrum. This was done with a copper 'through', a simple copper cable, at 4 Kelvin with all three covers, see figure 4.3. As expected the covers do not significantly alter the transmission spectrum in this case.

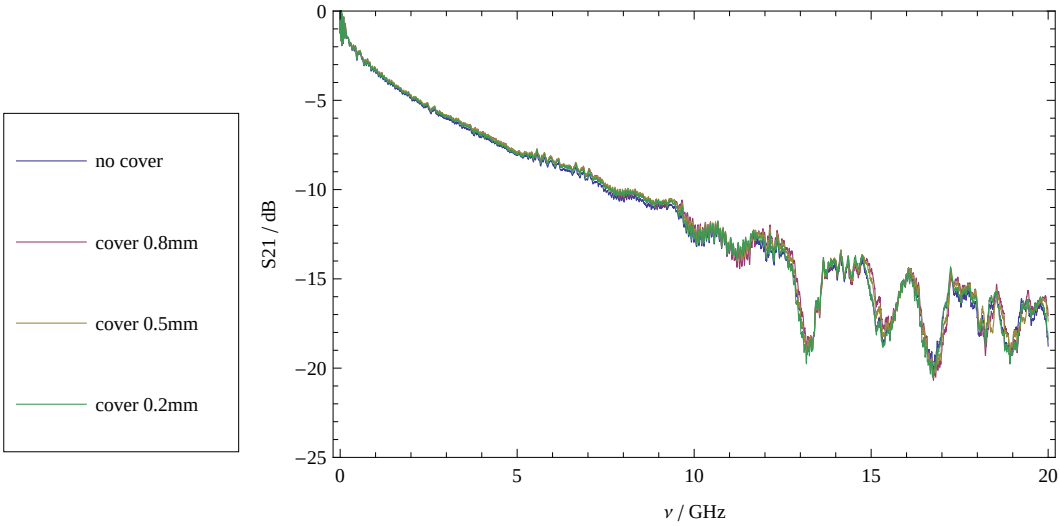

Figure 4.3.: Transmission spectrum for a copper 'through' at 4 Kelvin.

The use of the covers improves the spectrum quite a lot by suppressing unwanted resonances up to about 16GHz, see figure 4.4 for measurements with the copper resonator. The biggest improvement is achieved for the peaks near B and D. The copper resonator couples more strongly to its environment due to its different geometry in comparison to the niobium resonators. This shifts the resonance peaks of the copper resonator towards higher frequencies. In the case of the 0.2mm cover this shift is of the order of 200Mhz for the first resonator peak near 6GHz (A), 400MHz for the first harmonic near 12GHz (C) and 600MHz for the second harmonic near 18GHz (E).

The shift of resonance frequencies can be understood from the change of the effective dielectric constant due to the use of the cover. The copper of the cover has a different dielectric constant

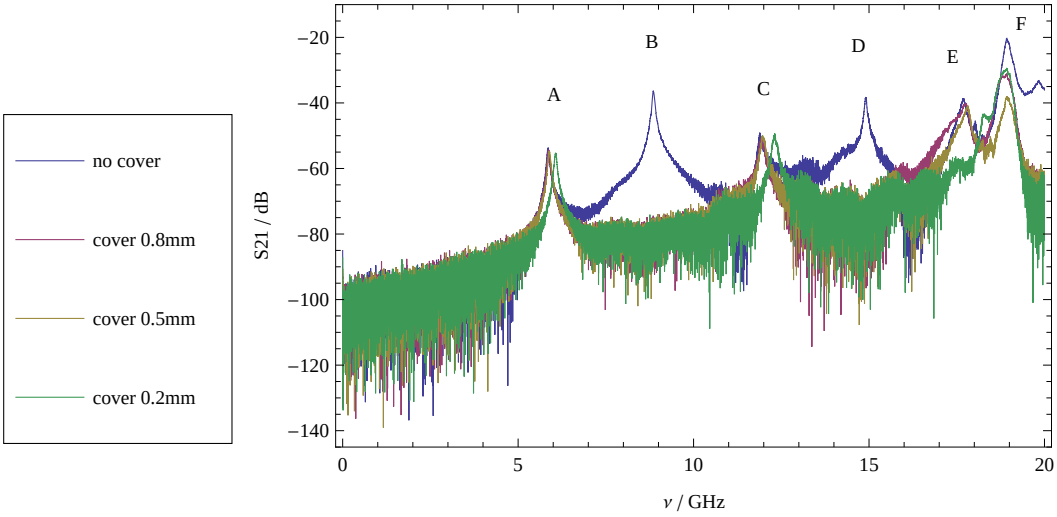

Figure 4.4.: Transmission spectrum for a copper resonator at room temperature.

letter	**no cover**		**cover 0.2mm**	
	ν/GHz	S21/dB	ν/GHz	S21/dB
A	5.85721	-53.7016	6.07121	-55.2365
B	8.85117	-36.3773		
C	11.8851	-49.0897	12.3091	-49.2827
D	14.9061	-38.2423		
E	17.6800	-38.5169	18.2820	-43.2355
	18.0210	-46.7743		
F	18.9240	-20.3581	18.9280	-29.4742
	19.8290	-33.1916		

Table 4.1.: Interesting peaks from figure 4.4.

than the air above the chip. Since in the vicinity of the chip there is more copper than without the use of the cover, the effective dielectric constant must change. The frequencies depend on the speed of light in the material and this depends on the dielectric constant. Therefore it is clear that the frequencies must shift.

The niobium resonator Tr07 equipped with the covers, shown in figure 4.5, shows similar behavior to the copper resonator discussed earlier. The resonance peaks of the sample itself are near 6.3GHz (A), near 12.7GHz (D) and near 19GHz (H). The main effect for the frequencies labeled B and C. At higher frequencies above 15GHz in the range from E to G the peaks are only marginally reduced. The peaks near G in the first three cases could be shifted to the left of the two frequencies near H where the sample was measured with the 0.2mm cover. The right peak near H is the second harmonic of A. The shifts of the resonator frequencies are on the order of 30MHz (A), 60MHz (D) and 120MHz (H) when using the 0.2mm cover. The positive value marked with (*) is not realistic since this would be an amplification of the signal. This is caused by the fact that the calibrated measurement is made with a copper 'through' but the measurement is done with a niobium resonator. The error of the measurement is then at least on the order of 1dB.

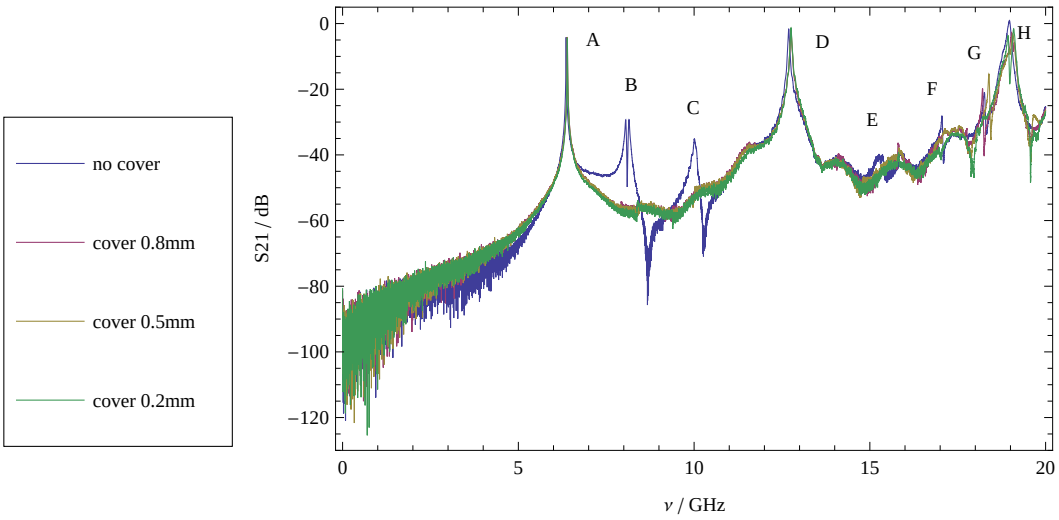

Figure 4.5.: Transmission spectrum for the niobium resonator Tr07 at 4 Kelvin.

letter	**no cover**		**cover 0.2mm**	
	ν/GHz	S21/dB	ν/GHz	S21/dB
A	6.36020	-4.15039	6.39420	-4.35711
B	8.05518	-29.2951		
	8.14718	-29.1955		
C	10.0111	-35.1518		
D	12.6921	-1.64704	12.7581	-1.26496
E	15.2581	-39.7056		
E	15.8741	-38.6683		
F	17.0550	-28.1428		
G	18.2580	-20.9910		
			18.9300	-3.80933
H	18.9700	+0.90463 (*)	19.0900	-1.73039

Table 4.2.: Interesting peaks from figure 4.5.

Finally with the second niobium resonator Tr01 from figure 4.6 improvements with the use of the covers are observable too. Frequencies in the range of 8GHz to 11GHz near C and E are significantly damped but also near G which is around 15GHz. The resonator is longer than the previous which leads to lower resonance frequencies. This is clearly visible. Resonances occur roughly every 3GHz (A, B, D, F, H, I) but just the odd integer multiples of A have sharp and high peaks. The even ones are damped stronger and spread wider. This could be in connection with the defect observed near the half length of the resonator, see figure 4.7.

For an open-circuited $\lambda/2$ transmission line the wavelengths λ_n that are possible for standing waves follow the equation $\lambda_n = 2l/n$ where l is the resonator length and n an integer bigger or equal than 1. The voltage has a minimum at half the resonator length $l/2$ for all odd numbers n, therefore the connection to ground at this location does not change the behavior of the circuit. We clearly see sharp peaks for n=1 (A, figure 4.6) and any other odd value of n (D,H). But for even values of n the voltage would have a maximum at the half length of

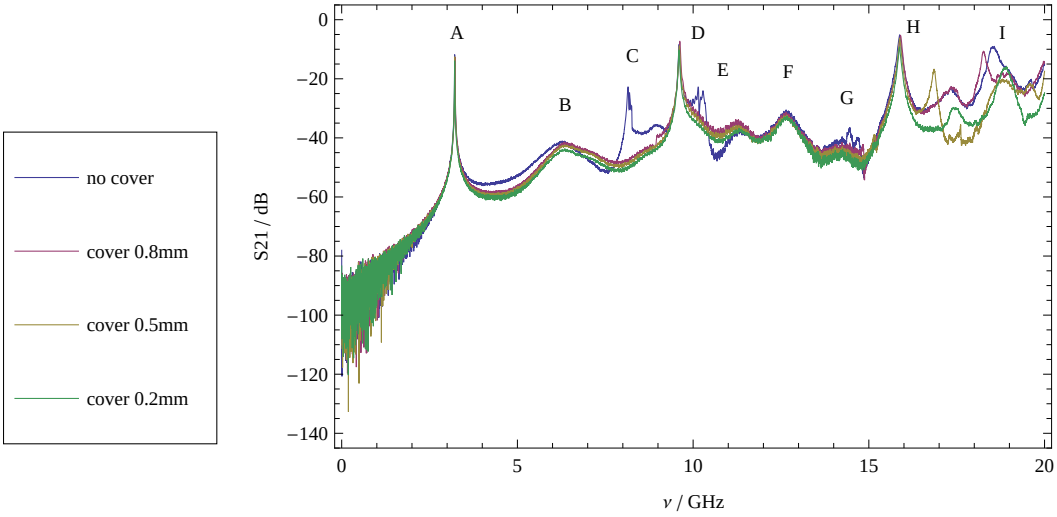

Figure 4.6.: Transmission spectrum for the niobium resonator Tr01 at 4 Kelvin.

letter	**no cover**		**cover 0.2mm**	
	ν/GHz	S21/dB	ν/GHz	S21/dB
A	3.21525	-11.7822	3.21325	-13.8839
B	6.27221	-41.2229	6.35320	-43.8807
C	8.14818	-22.7527		
C	9.00316	-35.6292		
D	9.60216	-8.34925	9.59916	-10.3207
E	10.1451	-22.7981		
E	10.2811	-24.0477		
F	12.6501	-30.5643	12.6681	-32.5596
G	14.4581	-36.4017		
H	15.8761	-5.21869	15.8761	-9.25942
I	18.5680	-9.15306	18.9200	-16.0703
	19.6110	-20.1977		

Table 4.3.: Interesting peaks from figure 4.6.

the resonator. This is not possible due to the ground connection, therefore we do not observe the sharp peaks for even n, see labels B and F in the same figure. This could explain the phenomenon that the resonances between the sharp peaks do not disappear with the use of the covers since they are modes of the niobium resonator itself.

This resonator was not the main test sample, it was just for further comparison and higher statistics of samples, a defect was known beforehand. Whether its influence makes the sample unusable for the purpose of this thesis was not known beforehand. This turned out not to be the case.

It is interesting that in any of the five measurements peaks appear in the neighborhood of 9GHz and 15GHz that are suppressed with the use of a cover. Examples are B and D in figure 4.4 and C, E and G in figure 4.6. For the niobium resonators they seem to be smaller, but in

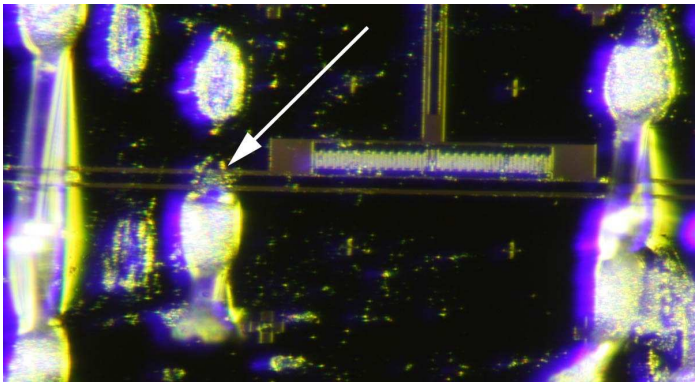

Figure 4.7.: Photograph of a possible defect of the niobium resonator Tr01 very close to half the resonator length. There the resonator could be connected to ground.

fact they have a comparable magnitude of about -30dB to -40dB. The 15GHz resonance has a wavelength of about 2cm which is on the scale of the sample. It is not completely suppressed when using only one cover which does not fill the the complete sample holder, see figures 3.2 and 3.3. If it would be a rectangular box mode it should probably be damped since less signal can get through when using a cover. Therefore it is thought of not appearing in the cavity above the chip and the signal lines.

Furthermore it is interesting to note that near 19GHz no complete reduction is achieved in any of the five measurements. This might correspond to effects in the remaining cavities of the covers. 19GHz correspond to roughly 1.6cm in wavelength which is a typical length scale of the sample. One suggestion might be that this is due to the cavity above the chip and signal line that goes straight through from the insertion connector, figure 4.2, to the connector for the transmitted signal since this distance is about this size. Another possibility is that the components of the measurement device are not designed for such high frequencies. At least the connectors are designed only for frequencies up to about 18 GHz.

In analyzing the different cover versions for all samples it is striking that below 16GHz they work almost equally good. Nevertheless the 0.2mm cover damps the peaks at frequencies above that range more than the other two versions. Therefore it should be the cover of choice if the shift of frequencies is not disturbing the experiment.

5. Analytic Calculations

As has been shown in chapter 2 about the theory of waveguides and resonators, one can derive the resonance frequencies for this electromagnetic problem from Maxwell's equations. Now they will be calculated explicitly for the particular geometry of the sample holder and the covers. Therefore we recall the resonance frequency equations of the TE_{nml} and TM_{nml} modes from a box resonator

$$f_{nml} = \frac{c}{2\sqrt{\mu_r \epsilon_r}} \sqrt{\left(\frac{m}{a}\right)^2 + \left(\frac{n}{b}\right)^2 + \left(\frac{l}{d}\right)^2}, \tag{5.1}$$

both equal with n=0,1,2,..., m=0,1,2,... and l=0,1,2,... and the constraint that n=m=l=0 is not allowed.
For the cylinder resonator it is

$$f_{nml} = \frac{c}{2\pi\sqrt{\mu_r \epsilon_r}} \sqrt{\left(\frac{p'_{nm}}{a}\right)^2 + \left(\frac{l\pi}{d}\right)^2} \tag{5.2}$$

for TE_{nml} and

$$f_{nml} = \frac{c}{2\pi\sqrt{\mu_r \epsilon_r}} \sqrt{\left(\frac{p_{nm}}{a}\right)^2 + \left(\frac{l\pi}{d}\right)^2} \tag{5.3}$$

for the TM_{nml} modes. Here n=0,1,2,... and l=0,1,2,... but m=1,2,3,... since m counts the roots of J_n and J'_n respectively. The first approximate values of these roots are summarized in tables 5.1 and 5.2.

n	p_{n1}	p_{n2}	p_{n3}
0	2.405	5.520	8.654
1	3.832	7.016	10.174
2	5.135	8.417	11.620

Table 5.1.: The first few roots of the Bessel function of first kind J_n.

n	p'_{n1}	p'_{n2}	p'_{n3}
0	3.832	7.016	10.174
1	1.841	5.331	8.536
2	3.054	6.706	9.970

Table 5.2.: The first few roots of the first derivative of the Bessel function of first kind J'_n.

The dimensions necessary for calculation are obtained from the sample holder and cover geometry and are as follows for the box resonator:

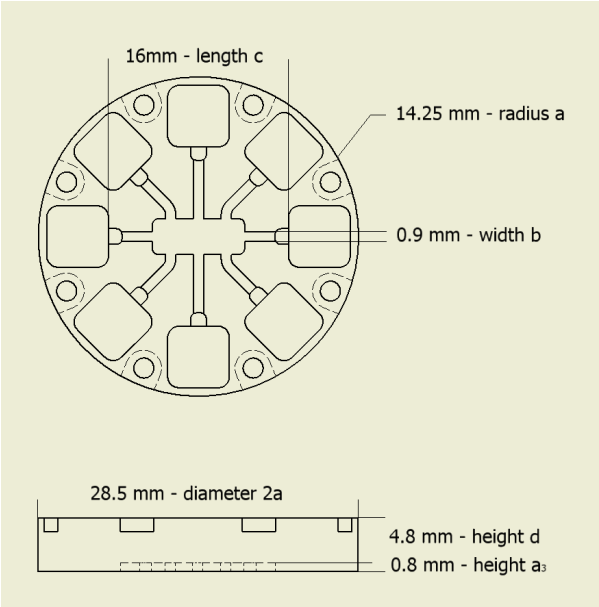

Figure 5.1.: The dimensions of the cover used for the calculations.

$$\begin{aligned} \text{height 1} \quad & a_1 = 0.2 \text{ mm}, \\ \text{height 2} \quad & a_2 = 0.5 \text{ mm}, \\ \text{height 3} \quad & a_3 = 0.8 \text{ mm}, \\ \text{width} \quad & b = 0.9 \text{ mm}, \\ \text{length} \quad & c = 16 \text{ mm}. \end{aligned}$$

The three heights given are the heights above the chip and the signal lines of the three different covers. For the cylinder resonator the constants are

$$\begin{aligned} \text{radius} \quad & a = 14.25 \text{ mm}, \\ \text{height} \quad & d = 4.8 \text{ mm}. \end{aligned}$$

Now it is to implement these constants and compare the resulting frequencies with the curves from the measurement section. Since the spectrum extends up to 20GHz, only frequencies smaller or equal to this are considered. For the box resonator this gives only two frequencies for the TE_{nml} and TM_{nml} modes in the range from 0 to 20GHz

n	m	l	ν/GHz
0	0	1	9.3685
0	0	2	18.737

Table 5.3.: Calculated frequencies of the box resonator.

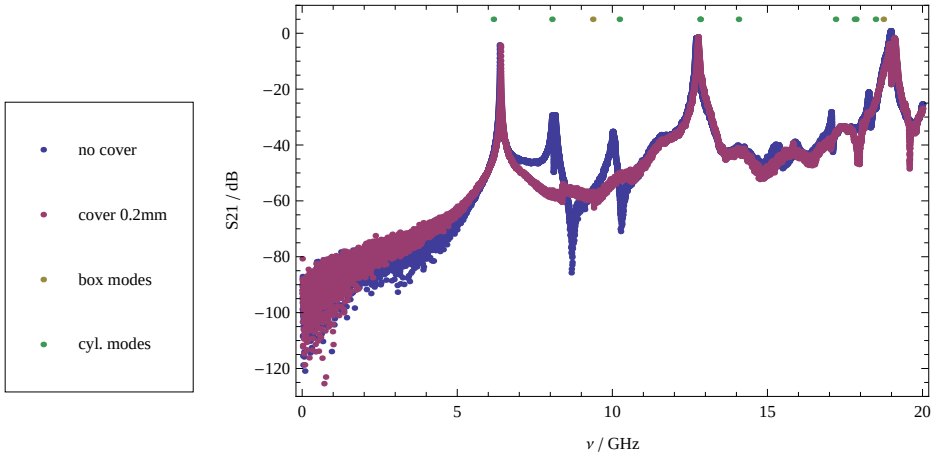

Figure 5.2.: The calculated frequencies together with the transmission spectrum of the niobium resonator Tr07.

Since the size of the a_i and b are so small, the corresponding frequencies would lie way beyond 20GHz such that only the length of the box plays a role. Therefore 'n' and 'm' are 0 in the frequency range used.
The calculation of resonance frequencies for the cylindrical resonator with the radius 'a' and the height 'd' leads to the frequencies from table 5.4.

n	m	l	ν/GHz	mode
1	1	0	6.16491	TE
0	1	0	8.05211	TM
2	1	0	10.2264	TE
0	1	0	12.8297	TE
1	1	0	12.8297	TM
3	1	0	14.0669	TE
2	1	0	17.1957	TM
4	1	0	17.8047	TE
1	2	0	17.8512	TE
0	2	0	18.4829	TM

Table 5.4.: Calculated frequencies of the cylinder resonator.

l=0 for the frequency range used, since as before the height of the cavity is so small that the frequencies would be out of range. To compare theory with experiment the calculated frequencies of the box and cylinder resonator are combined with the measurement in a single plot (figure 5.2).
Comparison of the frequencies from figure 5.2 can be done with tables 4.2 from the measurements with tables 5.3 and 5.4 from the calculations for the niobium resonator Tr07. Under the assumption that the first unwanted peak is not hidden by the first resonator peak, we observe from figure 5.2 that the very first frequency calculated does not coincide with the first unwanted peak. The first resonance frequency is then expected to be about 8 GHz and not about 6 GHz. Therefore one can introduce effective parameters. By doing so we obtain frequencies listed in tables 5.5 and 5.6 or visually in figure 5.3. The effective parameters used are:

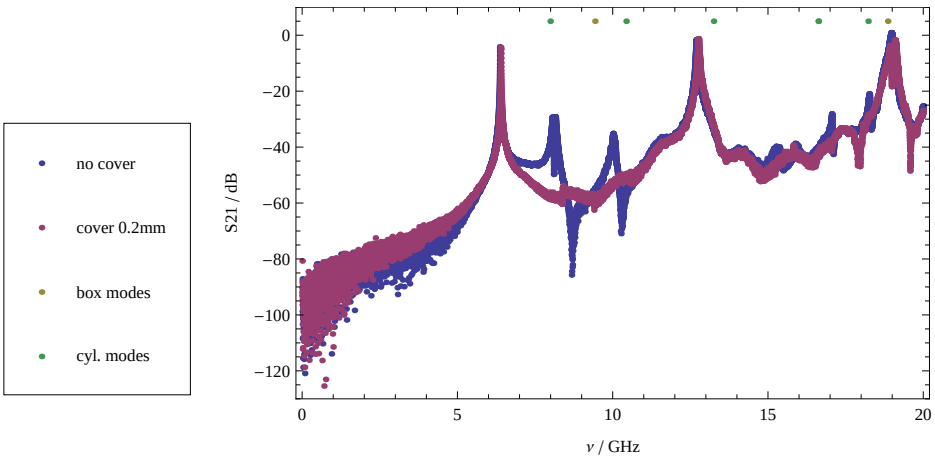

Figure 5.3.: The calculated optimized frequencies together with the transmission spectrum of the niobium resonator Tr07.

$$\text{effective box length} \quad c = 15.9 \text{ mm}$$
$$\text{effective cylinder radius} \quad a = 11 \text{ mm}$$

The effective box length c is less than 1% smaller, the effective cylinder radius roughly 23%.

n	m	l	ν/GHz
0	0	1	9.42744
0	0	2	18.8549

Table 5.5.: Calculated optimized frequencies of the box resonator for the niobium resonator sample.

n	m	l	ν/GHz	mode
1	1	0	7.98636	TE
0	1	0	10.4311	TM
2	1	0	13.2479	TE
0	1	0	16.6203	TE
1	1	0	16.6204	TM
3	1	0	18.2231	TE

Table 5.6.: Calculated optimized frequencies of the cylinder resonator for the niobium resonator sample.

The optimization shifts the first calculated frequency near the first unwanted peak from the spectrum around 8 GHz. The second unwanted peak near 10GHz is matched too by a TM mode. The last two calculated frequencies in the range used around 16GHz and 18GHz can also be related to the measurements. At around 19GHz the second box mode matches with the left of the two spikes.

For comparison with another sample we choose the copper resonator and use the original

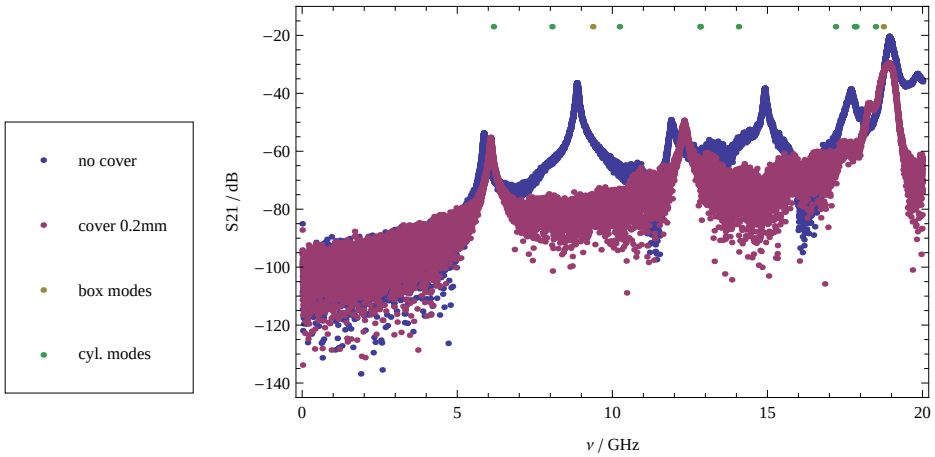

Figure 5.4.: The calculated frequencies together with the copper resonator.

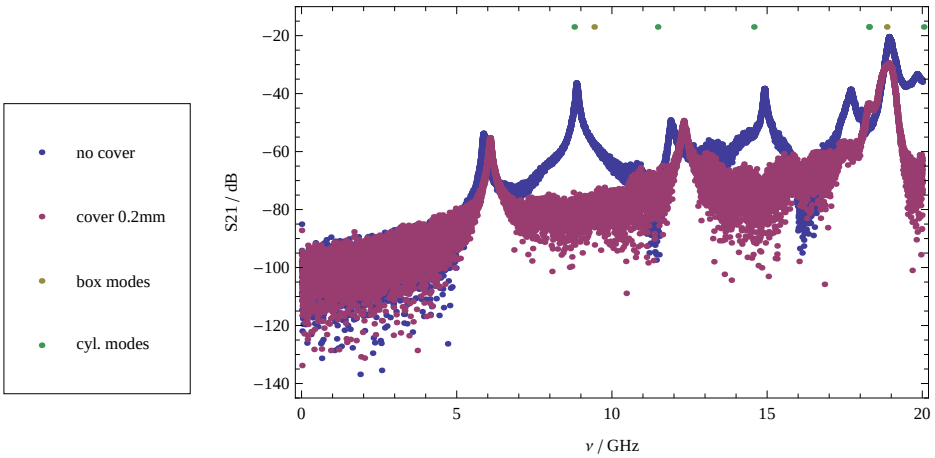

Figure 5.5.: The calculated optimized frequencies together with the copper resonator.

parameters see figure 5.4. The optimization is done separately, see figure 5.5 with the effective parameters given below. The frequency table for the optimized version are tables 5.7 and 5.8. The optimized parameters used are

$$\begin{aligned} \text{effective box length} \quad & c = 15.9 \text{ mm}, \\ \text{effective cylinder radius} \quad & a = 10 \text{ mm}, \end{aligned}$$

which is not far away from the parameters of niobium mentioned before. The effective box length is again less than 1% shorter than the originally assumed box length and the effective cylinder radius is roughly 30% shorter than the original value.The optimization of the spectrum for the copper resonator shifts the first calculated frequency towards the big peak near 9GHz which is between the first two copper resonator peaks. Also the second big spike near 15GHz which disappears with the use of the covers is closely matched by a TE mode. At last the spike near 20GHz is also in good agreement with the observation.

n	m	l	ν/GHz
0	0	1	9.42744
0	0	2	18.8549

Table 5.7.: Calculated optimized frequencies of the box resonator for the copper resonator sample.

n	m	l	ν/GHz	mode
1	1	0	8.7850	TE
0	1	0	11.4743	TM
2	1	0	14.5726	TE
0	1	0	18.2824	TE
1	1	0	18.2824	TM
3	1	0	20.0454	TE

Table 5.8.: Calculated optimized frequencies of the cylinder resonator for the copper resonator sample.

As we have seen the optimization procedures give reasonable predictions of the locations of the modes. But since the model is simplified and does not represent the exact geometry there is still an offset. The sample holder cavity is not exactly a completely hollow cylinder for example. Therefore deviations from the predictions are expected.

6. Results and conclusions

As has been demonstrated in the previous analysis of the cryostat sample holder the use of a cover is recommended for the experiment. Measurements in this project have shown that a well designed cover can damp unwanted modes significantly.

In the very beginning a first test with the existing covers was very promising since the unwanted peaks disappeared. This drove the design towards enlarging the height of the cover since this was effectively the only change in the very first test. Further optimization had less impact on the optimization of the sample holder.

Clearly visible in the spectra of the measurement samples is the vanishing of undesired resonances up to 16 GHz (between the actual resonances from the resonator on the sample) with any of the designed covers and little disturbance of the desired resonances. The version of the cover which goes closest to the chip and the signal lines, the 0.2mm version, shifts the resonances significantly towards higher frequencies. If this can be accepted, it should be used.

In calculating the cavity modes of a cylinder and a box resonator from Maxwell's equations the analytical frequencies do not match perfectly with the resonance peaks of the measured transmission spectra, thus effective cavity parameters have been introduced to improve the adjustment. It was found that the cylindrical cavity is effectively smaller in radius than the designed one of 14.25mm, namely around 10-11mm. This could be because the cavity is not empty since there are signal connectors on the sample.

Building on the success of the measurements shown here, experiments can now proceed to characterize the effect of using the designed covers in real qubit experiments. The design can also be modified for use with other device designs with different geometry. The effect of using a cover made from aluminum could also be analyzed at cryogenic temperatures.

A. Acknowledgment

I would like to thank Professor Dr. Andreas Wallraff for giving me the opportunity to carry out my semester thesis in his research group and to get an insight into the interesting topics the team is focusing on.
Special gratitude goes to my supervisor Dr. Stefan Filipp for guiding me into the topic of the thesis and the help he gave me when I got lost with something.
I enjoyed the nice group atmosphere and the helpfulness of all the colleagues.

Bibliography

[1] Michael A. Nielsen and Isaac L. Chuang, *Quantum Computation and Quantum Information*. Cambridge University Press, 2000.

[2] David M. Pozar, *Microwave Engineering*. John Wiley & Sons, Inc., third edition, 2005.

List of Figures

List of Tables